THE JOURNAL OF PHYSICAL CHEMISTRY C

pubs.acs.org/JPCC Article

Ammonia-Induced Seed Layer Transformations in a Hydrothermal Growth Process of Zinc Oxide Nanowires

Quanli Liu, Takao Yasui,* Kazuki Nagashima,* Takeshi Yanagida, Mitsuo Hara, Masafumi Horiuchi, Zetao Zhu, Hiromi Takahashi, Taisuke Shimada, Akihide Arima, and Yoshinobu Baba*

Cite This: J. Phys. Chem. C 2020, 124, 20563−20568 Read Online

ACCESS | Metrics & More | Article Recommendations | Supporting Information

ABSTRACT: Ammonia is a well-known additive to promote crystal growth in hydrothermal synthesis of ZnO nanowires. Although the effect of ammonia on the nanowire growth has been intensively investigated, its influence on the seed layer, which governs the initial nanowire growth, is rarely discussed. Here, we demonstrate that ammonia strongly affects the seed layer as well as the following nanowire growth. On increasing the ammonia concentration, the nanowire density first increases and then decreases, while the nanowire growth rate keeps increasing. Experimental results and thermodynamic calculations of the initial growth process reveal that the transformation of the seed layer induced by ammonia prior to nucleation critically determines the nanowire density and thus also influences the following nanowire growth. Present results highlight the critical importance of discussing the variation of seed layers in ammonia-involved hydrothermal synthesis and suggest a novel seed engineering approach for tailoring the ZnO nanowire growth.

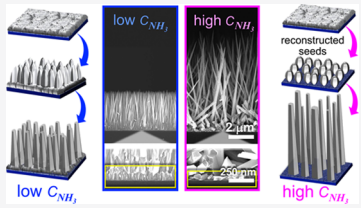

1. INTRODUCTION

The application field of single-crystalline zinc oxide (ZnO) nanowires has recently been extended from the previous optics and electronics to the newly emerging nano-bio analysis due to their various fascinating features including the wide direct band gap,[1,2] large exciton binding energy,[1−3] piezoelectricity,[4,5] Lewis acidity,[6,7] high isoelectric point,[8] and biocompatibility.[9,10] Thanks to such a variety of features, unique devices including light-emitting diodes (LEDs), nanogenerators, biochemical sensors, and biomedical analysis devices have been developed so far using ZnO nanowires.[11−15] A hydrothermal synthesis is among the most broadly utilized techniques for fabricating ZnO nanowires.[16−18] This is because the hydrothermal process is conducted at a temperature of less 100 °C and the diameter and position of nanowires are designable via seed crystals. These allow us to integrate ZnO nanowires with various materials and devices on a substrate.[19,20] Fundamentally, the anisotropic crystal growth of ZnO nanowires originates from a preferential nucleation on the ZnO(0001) plane, which is dominated by zinc hydroxide complex ($Zn(OH)_n$) precursors.[21−23] Ammonia is a well-known additive to promote the growth of ZnO nanowires.[24−28] Such an effect of ammonia has been interpreted in terms of the variations of ionic species in aqueous solution and their electrostatic interactions with ZnO crystal planes.[22,29] A recent study by Sakai et al. has further revealed that the increase of growth rate is mainly due to the change of the rate-limiting process from the precursor diffusion process to the ligand-exchange process, which is caused by the decreased concentration of $Zn(OH)_n$.[21] On the other hand, ammonia causes a dissociation of ZnO during the nanowire growth. Sharp and uniformly-shaped nanowire tips are formed as a result of ammonia-induced face-selective etching on ZnO(10$\bar{1}$1) planes.[30,31] Using this etching effect, Zhao et al. demonstrated the synthesis of monodisperse ZnO nanowires from randomly sized seeds.[31] The role of ammonia on the nanowire growth has been intensively investigated as described above, however, its influence on seeds, which govern the nanowire growth, is rarely discussed. Clarifying how ammonia influences the seeds is of crucial importance to comprehensively understand and tailor the ammonia-induced ZnO nanowire growth. Thus, in this study, we investigated the effect of ammonia on seeds in hydrothermal synthesis of ZnO nanowires. We found that ammonia transformed the seed layer prior to nucleation and strongly affected the following nanowire growth.

2. EXPERIMENTAL SECTION

ZnO nanowire growth was conducted by a hydrothermal synthesis. First, 20 mm × 10 mm silicon substrates (N-type) were cleaned in a mixture of 98% sulfuric acid and 35% hydrogen peroxide with a volume ratio of 3:1 at 180 °C for 2 h. After cooling down to room temperature, the substrates were taken out from the cleaning solution, washed with ultrapure water, and dried by blowing nitrogen gas. The ZnO seed layer

Received: June 17, 2020
Revised: August 25, 2020
Published: August 25, 2020

https://dx.doi.org/10.1021/acs.jpcc.0c05490
J. Phys. Chem. C 2020, 124, 20563−20568

was then deposited on the substrate by radio frequency (RF) sputtering with an RF power of 50 W under an ambient pressure of 1 Pa with an Ar/O_2 ratio of 5:1 at room temperature. The deposition rate of the ZnO seed layer was 10 nm/min. The thickness of ZnO seed layer was controlled to be 75 nm, where the highest areal density of uniformly shaped nanowires was available (see Supporting Information Figure S1). The nanowire growth solution was prepared by mixing zinc nitrate hexahydrate ($Zn(NO_3)_2{\cdot}6H_2O$, 40 mM), hexamethylenetetramine (HMTA, 40 mM), and ammonia solution (25 wt %) with varying concentrations in the range of 0−1000 mM at room temperature. The seed layer coated substrates were immersed into Teflon cups filled with 50 mL of growth solution in an upside down manner. Then, the Teflon cups were put into an oven was set at 95 °C. The growth time was varied between 10 and 180 min. After the growth, the samples were washed with ultrapure water and acetone and then dried at 80 °C for 10 min. The morphologies of the ZnO seed layer and ZnO nanowires were evaluated by scanning electron microscopy (SEM; Zeiss Supra 40 VP). The ZnO nanostructures constructed at an early stage were characterized by grazing incidence X-ray diffraction (GI-XRD; Rigaku FR-E). For GI-XRD, a radiation source of Cu Kα (λ = 0.154 nm) was used and the incident angle of the beam to the sample surface was adjusted at about 0.18−0.22°.

3. RESULTS AND DISCUSSION

Figure 1A shows the cross-sectional SEM images of ZnO nanowires grown for 3 h with varying ammonia concentrations (C_{NH_3}) of 0−1000 mM. Upon increasing C_{NH_3}, the nanowire growth rate increases. The observed trend is consistent with many previous studies, which can be interpreted in terms of the variations of ionic species in aqueous solution, their electrostatic interactions with ZnO crystal planes, and the rapid ligand-exchange process between different zinc complexes.[21−28] On the other hand, the areal number density of nanowires (hereafter, nanowire density) and the diameter show unique trends as explained in the following. Figure 1B shows the quantitative C_{NH_3} dependence on the nanowire density and the diameter. We found that the nanowire density tends to first increase and then decrease with increasing C_{NH_3}, and the diameter inversely correlates with the nanowire density. These trends cannot be explained by the ammonia-induced crystal growth promotion. Although the diameter is affected by various factors, the observed correlation indicates that the diameter is predominantly determined by a material competition effect between adjacent nanowires.[32] Thus, these results show that ammonia affects not only the nanowire growth rate but also the nanowire density and the diameter.

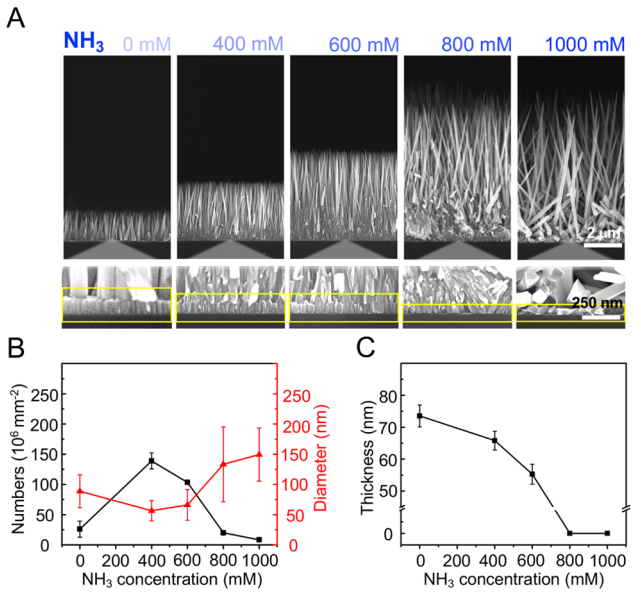

Figure 1. SEM images and statistical analysis of nanowires grown in various concentrations of ammonia after growth time for 3 h. (A) Nanostructure morphology variation along the horizontal direction with increase of ammonia concentration. Yellow squares are enlarged views of nanowire roots. Images in the same row use the same scale bars. (B) Nanowire areal density and diameter in various concentrations of ammonia. Error bars show the standard deviation for a series of measurements (for nanowire number: N = 10, for diameter: N = 100). (C) Thickness of the ZnO seed layer in various concentrations of ammonia. Error bars show the standard deviation for a series of measurements (N = 3).

We found that the seed layer located at the bottom of nanowires tends to be thinner with increasing C_{NH_3}, as shown in Figure 1A,C. This result indicates the significant effect of ammonia on the seed layer and therefore strongly recommends observation of the seed layer at the initial growth process, although has rarely been discussed previously. Figure 2A shows SEM images of the seed layer observed after 10−30 min of growth process with various C_{NH_3}. At a relatively low C_{NH_3} in the range of 0−600 mM, the nanowire growth immediately occurs within 20 min. In this condition, the nanowire density tends to increase with increasing C_{NH_3}. On the other hand, in a relatively high C_{NH_3}range of 800−1000 mM, the seed layer seems to be removed from the substrate and no nanowire growth can be seen. We found that the seed layer is removed within the first 10 min and the nanoparticles tend to form in the following 20 min. The variations of nanowire and nanoparticle density observed at the initial growth process is consistent with that of the nanowire density in Figure 1B, suggesting that the nanowire density is determined by the morphology of the seed layer formed at the initial growth process. Thus, the result in Figure 2A clearly reveals that ammonia strongly affects the seed layer at initial growth process, as well as the following nanowire growth.

Here, we consider how ammonia affects the seed layer at the initial growth process. First, we discuss the increasing trend of nanowire density with increasing C_{NH_3} in a relatively low concentration range. Since the seed layer fully covers the substrate in this C_{NH_3} range, the variation of nanowire density is determined by the nucleation phenomena on the seed layer. As seen in Figure 1A, a nanowire is grown from several seed crystals at C_{NH_3} 0 mM, while it tends to grow from an individual seed crystal by increasing C_{NH_3}. This trend can be interpreted in terms of the suppression of merging of nuclei via ammonia-induced sharp tip formation as demonstrated by our previous study.[31] When using the densely deposited seed crystals, the adjacent nuclei spontaneously merge during the nanowire growth, leading to the decrease of nanowire density. In the previous study, we found that the sharp tip seeds formed by ammonia-based etching provided the spatially separated nucleation sites and suppressed the merging of nuclei. Since the sharp tip formation on seeds is promoted by increasing

https://dx.doi.org/10.1021/acs.jpcc.0c05490
J. Phys. Chem. C 2020, 124, 20563−20568

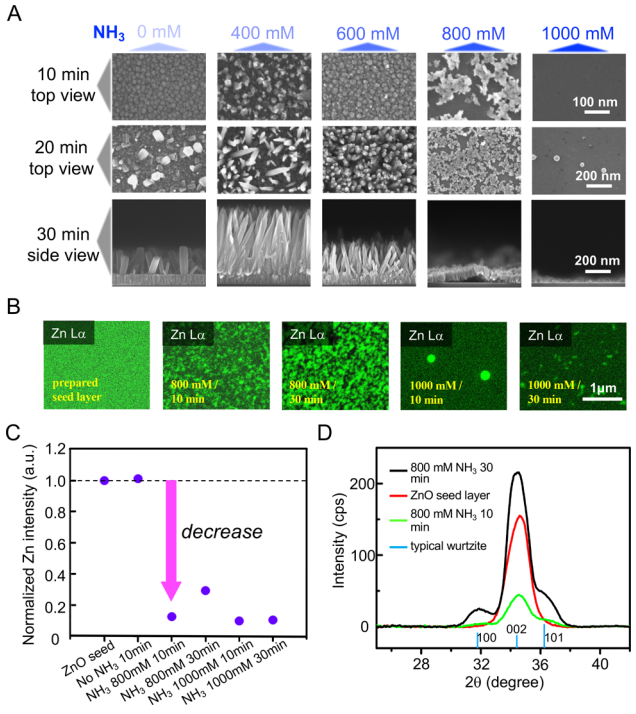

Figure 2. Characteristics of ZnO seed layers. (A) SEM images of synthesis products at the initial 10, 20, and 30 min. Product morphologies vary with increase of ammonia concentrations. Images in the same row have the same scale bar as given in the last image of the row. (B) Energy dispersive spectroscopy (EDS) mapping analysis of seed layer transformation after immersing into growth solution with 800 and 1000 mM ammonia for 10 and 30 min, respectively. Images have the same scale bar as given in the last image of the row. (C) Normalized Zn intensity of the substrate during the initial 30 min of the hydrothermal process. (D) GI-XRD profiles of the prepared ZnO seed layer and after immersing it into growth solution with 800 mM ammonia for 10 and 30 min. Vertical light blue lines indicate typical wurtzite (JCPDS No. 36-1451) peak positions.

C_{NH_3}, this might lead to an increase in nanowire density in a relatively low concentration range.

Second, we discuss the decreasing trend of nanowire density with increasing C_{NH_3} in a relatively high concentration range. According to the results in Figure 1C and Figure 2A, we assume that the seed layer is dissociated prior to the nucleation, and the number of remaining seeds might determine the nanowire density. In fact, the pH becomes over 11 by introducing 800 mM ammonia (see Supporting Information Figure S2), which is high enough for dissociating ZnO.[31,33] Figure 2B shows the Zn mapping of seed layers characterized by energy-dispersive spectroscopy (EDS). The images are taken from the initial seed layer, and after 10−30 min of growth process with various C_{NH_3} (all data are shown in Supporting Information Figure S3). We found that the seeds are inhomogeneously distributed at C_{NH_3} 800 mM, and only sparsely distributed nanoparticles are seen at C_{NH_3} 1000 mM. More specifically, the relative Zn intensity normalized by the initial ZnO seed layer decreases by 88−90% after 10 min of the growth process at C_{NH_3} 800−1000 mM (Figure 2C). These results clearly reveal that the seed layer is dissociated during the initial growth process in a relatively high C_{NH_3} range.

We also found in Figure 2B that the seed density increases by extending the growth time to 30 min, which is consistent with the result in Figure 2A and confirmed by the variation of Zn intensity in Figure 2C. To specify the variation of seed crystals observed above, we performed GI-XRD measurements with varying growth time in Figure 2D. In this experiment, the samples of C_{NH_3} 800 mM were evaluated. Two trends were found as to the variation of seed crystals. First, on increasing the growth time, the ZnO(002) peak intensity initially decreased at 10 min and then increased at 30 min consistent with results in Figure 2A−C. This indicates that the seed crystals are reconstructed after the dissociation. Second, although only the ZnO(002) peak is observable in the initial seed layer, the (100) peak and the (101) peak also tend to appear with increasing growth time, showing that variously oriented seed crystals are reconstructed after the dissociation. Such reconstructed seed crystals led to a variety of orientation in the nanowires grown at high C_{NH_3} conditions (see Figure 1A). It should be noted that the seed density at 30 min of growth time is very similar to that observed in Figure 1A. Thus, these results highlight that the nanowire density at high C_{NH_3} conditions is strongly governed via dissociation and reconstruction of the seed crystals.

To gain an in-depth insight into the experimental results observed above, we performed thermodynamic calculations at the given growth conditions. In this calculation, the solubility of ZnO, i.e., the saturated Zn concentration, was estimated by involving all of the related zinc ions that existed in the growth solution. The details of the calculation are provided in Supporting Information S4. The pH value and the temperature of growth solution were measured at each growth time and utilized for estimating the solubility (see Supporting Information Figure S2). Figure 3A,B shows the pH-dependent

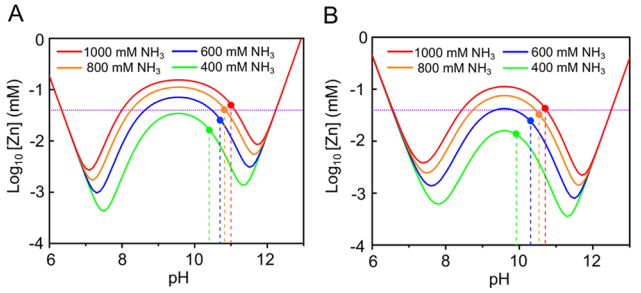

Figure 3. pH value-dependent theoretical solubility of Zn(II) in aqueous solutions with varied concentrations of ammonia. (A) pH value-dependent theoretical solubility of Zn(II) in aqueous solutions with varied concentrations of ammonia at 25 °C. (B) pH value-dependent theoretical solubility of Zn(II) in aqueous solutions with varied concentrations of ammonia at 60 °C. Intersection points of the solid curve and the dashed line in the same color represent theoretical solubility of Zn(II) at corresponding measured pH values. Horizontal dotted line represents Zn(II) concentration in the prepared aqueous solution, which is equal to zinc nitrate hexahydrate concentration, 40 mM.

solubility of ZnO with various C_{NH_3} at 25 and 60 °C, respectively, where 60 °C is associated with the growth time of 10−20 min. Note that the dotted lines and the filled circles in the figures represent the Zn concentration used for the nanowire growth and the solubility of ZnO at the measured pH conditions, respectively. In a relatively low C_{NH_3} range (i.e.,

https://dx.doi.org/10.1021/acs.jpcc.0c05490
J. Phys. Chem. C 2020, 124, 20563−20568

400−600 mM), the growth solution is almost saturated at 25 °C and supersaturated at 60 °C. This result shows good consistency with the results of Figure 2A, of which the nanowire growth immediately occurs after 10 min of growth time at this condition. In contrast, in a relatively high C_{NH_3} range (i.e., 800−1000 mM), the growth solution is not saturated and affords dissociation of ZnO at 25 °C, while it becomes supersaturated on increasing the temperature up to 60 °C. Such a temperature dependence observed in the higher C_{NH_3} range is consistent with a previous study, where $Zn(NH_3)_4^{2+}$ ions dominate the solubility of ZnO in ammonia-added aqueous solution.[21] In fact, our calculations reveal that the solubility of ZnO in our experimental conditions is governed by the concentration of $Zn(NH_3)_4^{2+}$ ions (see Supporting Information Figure S5). Thus, the dynamic change of saturation degree induced by temperature variation reasonably explains why the seed layer is dissociated at first and then reconstructed during the initial growth process.

4. CONCLUSIONS

In conclusion, we investigated the effect of ammonia on the seed layer in hydrothermal synthesis of ZnO nanowires, which had been rarely discussed previously. The nanowire growth rate increase accompanying the increase of C_{NH_3} is consistent with many previous studies. On the contrary, the nanowire density and the diameter exhibited unique tendencies, of which the nanowire density first increased and then decreased with increasing C_{NH_3} and the diameter inversely correlated with the nanowire density. The detailed experimental analysis revealed that the transformation of the seed layer occured prior to the nucleation and critically determined the features of fabricated nanowires including the nanowire density and the diameter. We found that the nanowire density was governed by two dominant transformations of the seed layer, i.e., the formation of sharp tips on the seed increased the nanowire density by suppressing the merging of adjacent nuclei in a relatively low C_{NH_3} range and the dissociation of the seed layer decreased the nanowire density in a relatively high C_{NH_3} range. We also found that in a relatively high C_{NH_3} range, the seed crystals were reconstructed after the dissociation. Thermodynamic calculations revealed that the variation of saturation degree at the initial growth process is responsible for the reconstruction of seed crystals. Our results highlight that observing the variation of seed layers at the initial growth process is of critical importance to understand the comprehensive growth mechanism in ammonia-involved hydrothermal ZnO nanowire synthesis and also suggest a novel seed engineering approach for tailoring the ZnO nanowire growth.

■ ASSOCIATED CONTENT

Supporting Information

The Supporting Information is available free of charge at https://pubs.acs.org/doi/10.1021/acs.jpcc.0c05490.

SEM images, diameter and areal density of ZnO nanowires grown with various seed layer thicknesses. The data was taken with a growth time of 3 h and without NH_3 (Figure S1); pH value and temperature of growth solution over time (Figure S2); EDS mapping analysis of the seed layer on a silicon substrate after immersing into growth solution with varying ammonia concentration for 10 and 30 min, respectively (Figure S3); thermodynamic calculation of Zn(II) solubility in aqueous solutions (S4); speciation of dissolved Zn(II) versus pH and temperature in growth solution (Figure S5) (PDF)

■ AUTHOR INFORMATION

Corresponding Authors

Takao Yasui − *Department of Biomolecular Engineering, Graduate School of Engineering, Nagoya University, Nagoya 464-8603, Japan; Japan Science and Technology Agency (JST), Precursory Research for Embryonic Science and Technology (PRESTO), Kawaguchi, Saitama 332-0012, Japan;* orcid.org/0000-0003-0333-3559; Email: yasui@chembio.nagoya-u.ac.jp

Kazuki Nagashima − *Department of Applied Chemistry, School of Engineering, The University of Tokyo, Tokyo 113-8656, Japan;* orcid.org/0000-0003-0180-816X; Email: kazu-n@g.ecc.u-tokyo.ac.jp

Yoshinobu Baba − *Department of Biomolecular Engineering, Graduate School of Engineering, Nagoya University, Nagoya 464-8603, Japan; Health Research Institute, National Institute of Advanced Industrial Science and Technology (AIST), Takamatsu 761-0395, Japan*; Email: babaymtt@chembio.nagoya-u.ac.jp

Authors

Quanli Liu − *Department of Biomolecular Engineering, Graduate School of Engineering, Nagoya University, Nagoya 464-8603, Japan;* orcid.org/0000-0002-1684-7447

Takeshi Yanagida − *Department of Applied Chemistry, School of Engineering, The University of Tokyo, Tokyo 113-8656, Japan; Institute of Materials Chemistry and Engineering, Kyushu University, Kasuga, Fukuoka 816-8580, Japan; Institute of Scientific and Industrial Research, Osaka University, Ibaraki, Osaka 567-0047, Japan;* orcid.org/0000-0003-4837-5701

Mitsuo Hara − *Department of Molecular and Macromolecular Chemistry, Graduate School of Engineering, Nagoya University, Nagoya 464-8603, Japan;* orcid.org/0000-0003-1829-5153

Masafumi Horiuchi − *Department of Biomolecular Engineering, Graduate School of Engineering, Nagoya University, Nagoya 464-8603, Japan*

Zetao Zhu − *Department of Biomolecular Engineering, Graduate School of Engineering, Nagoya University, Nagoya 464-8603, Japan*

Hiromi Takahashi − *Department of Biomolecular Engineering, Graduate School of Engineering, Nagoya University, Nagoya 464-8603, Japan*

Taisuke Shimada − *Department of Biomolecular Engineering, Graduate School of Engineering, Nagoya University, Nagoya 464-8603, Japan*

Akihide Arima − *Department of Biomolecular Engineering, Graduate School of Engineering, Nagoya University, Nagoya 464-8603, Japan;* orcid.org/0000-0002-1914-5686

Complete contact information is available at: https://pubs.acs.org/10.1021/acs.jpcc.0c05490

Notes

The authors declare no competing financial interest.

https://dx.doi.org/10.1021/acs.jpcc.0c05490
J. Phys. Chem. C 2020, 124, 20563−20568

■ ACKNOWLEDGMENTS

This research was supported by PRESTO (JPMJPR151B, JPMJPR19H9), Japan Science and Technology Agency (JST), the "Development of Diagnostic Technology for Detection of miRNA in Body Fluids" grant from the Japan Agency for Medical Research and Development and New Energy and Industrial Technology Development Organization, the JSPS Grant-in-Aid for Young Scientists (A) 17H04803, the JSPS Grant-in-Aid for Scientific Research (A) 16H02091, the JSPS Grant-in-Aid for Scientific Research (S) 18H05243, a research grant from the Murata Science Foundation, Advanced Technology Institute Research Grants 2019, the Foundation of Public Interest of Tatematsu, the Nitto Foundation, and the Nanotechnology Platform Program (Molecule and Material Synthesis) of the Ministry of Education, Culture, Sports, Science and Technology (MEXT). We thank Dr. Daisuke Onoshima and Dr. Hiroshi Yukawa for valuable discussions.

■ REFERENCES

(1) Xu, S.; Wang, Z. L. One-dimensional ZnO nanostructures: Solution growth and functional properties. *Nano Res.* **2011**, *4*, 1013−1098.
(2) Özgür, Ü.; Alivov, Y. I.; Liu, C.; Teke, A.; Reshchikov, M. A.; Doğan, S.; Avrutin, V.; Cho, S. J.; Morkoç, H. A comprehensive review of ZnO materials and devices. *J. Appl. Phys.* **2005**, *98*, No. 041301.
(3) Thomas, D. G. The exciton spectrum of zinc oxide. *J. Phys. Chem. Solids* **1960**, *15*, 86−96.
(4) Wang, Z. L.; Song, H. Piezoelectric nanogenerators based on zinc oxide nanowire arrays. *Science* **2006**, *312*, 242−246.
(5) Groo, L.; Inman, D. J.; Sodano, H. A. In situ damage detection for fiber-reinforced composites using integrated zinc oxide nanowires. *Adv. Funct. Mater.* **2018**, *28*, No. 1802846.
(6) Ballerini, G.; Ogle, K.; Barthés-Labrousse, M.-G. The acid−base properties of the surface of native zinc oxide layers: An XPS study of adsorption of 1,2-diaminoethane. *Appl. Surf. Sci.* **2007**, *253*, 6860−6867.
(7) Perez-Lopez, O. W.; Farias, A. C.; Marcilio, N. R.; Bueno, J. M. C. The catalytic behavior of zinc oxide prepared from various precursors and by different methods. *Mater. Res. Bull.* **2005**, *40*, 2089−2099.
(8) Cao, L.; Kiely, J.; Piano, M.; Luxton, R. Facile and inexpensive fabrication of zinc oxide based bio-surfaces for C-reactive protein detection. *Sci. Rep.* **2018**, *8*, No. 12687.
(9) Dagdeviren, C.; Hwang, S.-W.; Su, Y.; Kim, S.; Cheng, H.; Gur, O.; Haney, R.; Omenetto, F. G.; Huang, Y.; Rogers, J. A. Transient, Biocompatible electronics and energy harvesters based on ZnO. *Small* **2013**, *9*, 3398−3404.
(10) Bhang, S. H.; Jang, W.; Han, J.; Yoon, J.-K.; La, W.-G.; Lee, E.; Kim, Y. S.; Shin, J.-Y.; Lee, T.-J.; Baik, H. K.; et al. Zinc oxide nanorod-based piezoelectric dermal patch for wound healing. *Adv. Funct. Mater.* **2017**, *27*, No. 1603497.
(11) Bao, J.; Zimmler, M. A.; Capasso, F.; Wang, X.; Ren, Z. F. Broadband ZnO single-nanowire light-emitting diode. *Nano Lett.* **2006**, *6*, 1719−1722.
(12) Wang, X.; Song, J.; Liu, J.; Wang, Z. L. Direct-current nanogenerator driven by ultrasonic waves. *Science* **2007**, *316*, 102−105.
(13) Haarindraprasad, R.; Hashim, U.; Gopinath, S. C. B.; Perumal, V.; Liu, W.-W.; Balakrishnan, S. R. Fabrication of interdigitated high-performance zinc oxide nanowire modified electrodes for glucose sensing. *Anal. Chim. Acta* **2016**, *925*, 70−81.
(14) Xu, X.; Yan, M.; Tian, X.; Yang, C.; Shi, M.; Wei, Q.; Xu, L.; Mai, L. In situ investigation of Li and Na ion transport with single nanowire electrochemical devices. *Nano Lett.* **2015**, *15*, 3879−3884.
(15) Yasui, T.; Yanagida, T.; Ito, S.; Konakade, Y.; Takeshita, D.; Naganawa, K.; Nagashima, K.; Shimada, T.; Kaji, N.; Nakamura, Y.; et al. Unveiling massive numbers of cancer-related urinary-microRNA candidates via nanowires. *Sci. Adv.* **2017**, *3*, No. e1701133.
(16) Cheng, J. J.; Nicaise, S. M.; Berggren, K. K.; Gradečak, S. Dimensional tailoring of hydrothermally grown zinc oxide nanowire arrays. *Nano Lett.* **2016**, *16*, 753−759.
(17) Cho, J.; Salleh, N.; Blanco, C.; Yang, S.; Lee, C.; Kim, Y.; Kim, J.; Liu, J. Novel synthetic methodology for controlling the orientation of zinc oxide nanowires grown on silicon oxide substrates. *Nanoscale* **2014**, *6*, 3861−3867.
(18) Qiu, J.; Li, X.; He, W.; Park, S.-J.; Kim, H.-K.; Hwang, Y.-H.; Lee, J.-H.; Kim, Y.-D. The growth mechanism and optical properties of ultralong ZnO nanorod arrays with a high aspect ratio by a preheating hydrothermal method. *Nanotechnology* **2009**, *20*, No. 155603.
(19) Ou, C.; Sanchez-Jimenez, P.; Datta, A.; Boughey, F. L.; Whiter, R. A.; Sahonta, S. L.; Kar-Narayan, S. Template-assisted hydrothermal growth of aligned zinc oxide nanowires for piezoelectric energy harvesting applications. *ACS Appl. Mater. Interfaces* **2016**, *8*, 13678−13683.
(20) Azzouz, I.; Habba, Y. G.; Capochichi-Gnambodoe, M.; Marty, F.; Vial, J.; Leprince-Wang, Y.; Bourouina, T. Zinc oxide nano-enabled microfluidic reactor for water purification and its applicability to volatile organic compounds. *Microsyst. Nanoeng.* **2018**, *4*, No. 17093.
(21) Sakai, D.; Nagashima, K.; Yoshida, H.; Kanai, M.; He, Y.; Zhang, G.; Zhao, X.; Takahashi, T.; Yasui, T.; Hosomi, T.; et al. Substantial narrowing on the Width of "concentration Window" of hydrothermal ZnO nanowires via ammonia addition. *Sci. Rep.* **2019**, *9*, No. 14160.
(22) He, Y.; Yanagida, T.; Nagashima, K.; Zhuge, F.; Meng, G.; Xu, B.; Klamchuen, A.; Rahong, S.; Kanai, M.; Li, X.; et al. Crystal-plane dependence of critical concentration for nucleation on hydrothermal ZnO nanowires. *J. Phys. Chem. C* **2013**, *117*, 1197−1203.
(23) Cossuet, T.; Appert, E.; Thomassin, J.-L.; Consonni, V. Polarity-dependent growth rates of selective area grown ZnO nanorods by chemical bath deposition. *Langmuir* **2017**, *33*, 6269−6279.
(24) Syrrokostas, G.; Govatsi, K.; Yannopoulos, S. N. High-quality, reproducible ZnO nanowire arrays obtained by a multiparameter optimization of chemical bath deposition growth. *Cryst. Growth Des.* **2016**, *16*, 2140−2150.
(25) Richardson, J. J.; Lange, F. F. Controlling low temperature aqueous synthesis of ZnO. 2. A novel continuous circulation reactor. *Cryst. Growth Des.* **2009**, *9*, 2576−2581.
(26) Kwon, T. H.; Kim, K.; Park, S. H.; Annamalai, A.; Lee, M. J. Effect of seed particle size and ammonia concentration on the growth of ZnO nanowire arrays and their photoconversion efficiency. *Int. J. Nanotechnol.* **2013**, *10*, 681−691.
(27) Boubenia, S.; Dahiya, A. S.; Poulin-Vittrant, G.; Morini, F.; Nadaud, K.; Alquier, D. A facile hydrothermal approach for the density tunable growth of ZnO nanowires and their electrical characterizations. *Sci. Rep.* **2017**, *7*, No. 15187.
(28) Chen, L.-Y.; Yin, Y.-T.; Chen, C.-H.; Chiou, J.-W. Influence of polyethyleneimine and ammonium on the growth of ZnO nanowires by hydrothermal method. *J. Phys. Chem. C* **2011**, *115*, 20913−20919.
(29) Richardson, J. J.; Lange, F. F. Controlling low temperature aqueous synthesis of ZnO. 1. Thermodynamic analysis. *Cryst. Growth Des.* **2009**, *9*, 2570−2575.
(30) Wang, H. Q.; Li, G. H.; Jia, L. C.; Wang, G. Z.; Li, L. General in situ chemical etching synthesis of ZnO nanotips array. *Appl. Phys. Lett.* **2008**, *93*, No. 153110.
(31) Zhao, X.; Nagashima, K.; Zhang, G.; Hosomi, T.; Yoshida, H.; Akihiro, Y.; Kanai, M.; Mizukami, W.; Zhu, Z.; Takahashi, T.; et al. Synthesis of monodispersedly sized ZnO nanowires from randomly sized seeds. *Nano Lett.* **2020**, *20*, 599−605.
(32) Lee, J. M.; No, Y.-S.; Kim, S.; Park, H.-G.; Park, W. I. Strong interactive growth behaviours in solution-phase synthesis of three-dimensional metal oxide nanostructures. *Nat. Commun.* **2015**, *6*, No. 6325.

https://dx.doi.org/10.1021/acs.jpcc.0c05490
J. Phys. Chem. C 2020, 124, 20563−20568

(33) Zhou, J.; Xu, N. S.; Wang, Z. L. Dissolving behavior and stability of ZnO wires in biofluids: A study on biodegradability and biocompatibility of ZnO nanostructures. *Adv. Mater.* **2006**, *18*, 2432−2435.

https://dx.doi.org/10.1021/acs.jpcc.0c05490
J. Phys. Chem. C 2020, 124, 20563−20568